Effect of the packing structure of silicon chunks on the melting process and carbon reduction in Czochralski silicon crystal growth

Liu, Xin
Research Institute for Applied Mechanics, Kyushu University

Han, Xue-Feng
Research Institute for Applied Mechanics, Kyushu University

Nakano, Satoshi
Research Institute for Applied Mechanics, Kyushu University

Kakimoto, Koichi
Research Institute for Applied Mechanics, Kyushu University : Professor

Effect of the packing structure of silicon chunks on the melting process and carbon reduction in Czochralski silicon crystal growth

Xin LIU[*1], Xue-Feng HAN[*1], Satoshi NAKANO[*1] and Koichi KAKIMOTO[*1]

E-mail of corresponding author: *liuxin@riam.kyushu-u.ac.jp*

(Received January 31, 2017)

Abstract

Carbon (C) contamination in Czochralski silicon (CZ-Si) crystal growth mainly originates from carbon monoxide (CO) generation on the graphite components, which reaches a maximum during the melting stage. Loading a crucible with poly-Si feedstock includes many technical details for optimization of the melting and growth processes. To investigate the effect of the packing structure of Si chunks on C accumulation in CZ-Si crystal growth, transient global simulations of heat and mass transport were performed for the melting process with different packing structures of poly-Si. The heat transport modeling took into account the effective thermal conductivity (ETC) of the Si feedstock, which is affected by the packing structure. The effect of the chunk size on the melting process and C accumulation were investigated by parametric studies of different packing structures. The heat transport and melting process in the crucible were affected by the ETC and the emissivity of the Si feedstock. It was found that smaller Si chunks packed in the upper part could speed up the melting process and smooth the power profile. Decreasing the duration of the melting process is favorable for reduction of C contamination in the Si feedstock. Parametric studies indicated that optimization of the melting process by the packing structure is possible and essential for C reduction in CZ-Si crystal growth.

Keywords: *Computer simulation, Impurities, Mass transfer, Czochralski method*

1. Introduction

The minority carrier lifetime of silicon (Si) wafers is one of the most important parameters in fabrication of power devices. The bulk lifetime of Si crystals is shortened by oxygen (O) precipitates, which are enhanced by carbon (C) contamination[1, 2]. Therefore, reduction of C contamination in Czochralski silicon (CZ-Si) crystal growth is required for production of Si wafer with a long carrier lifetime. Contamination of C in Si crystals mainly originates from carbon monoxide (CO) generation on the graphite components, which reaches a maximum in the melting stage[3]. It is essential to control CO generation and C incorporation from melting to tailing.

Loading a crucible with poly-Si feedstock includes many technical details for optimization of the melting and growth processes[4]. In the CZ-Si process, poly-Si in the form of granules, chunks, or a mixture of chunks and granules is first loaded into a quartz crucible. The packing density of poly-Si within the crucible is greater than about 0.7. For the melting of packed Si chunks, the packing structure can affect the heat transport by the effective thermal conductivity (ETC), which is different from the thermal conductivity of bulk Si. The ETC is a function of many parameters, including the conductivities of the solid and the fluid, porosity,

emissivity, temperature, and chunk size[5]. Many researchers have proposed ETC models according to different modeling principles[6]. Several models have the full-function definition, including contributions from conduction of the solid and the fluid, contact of spheres, and thermal radiation. They include the classic ZBS model[7] (proposed by Zehner, Bauer, and Schlunder in 1978) and the IAEA model[8] (applied by International Atomic Energy Agency in 2000). The IAEA model is a hybrid model based on several proposed models, and it was validated by the experimental data of the pebble bed.

Transport phenomena of C as well as relevant impurities and species in the CZ-Si process have been extensively studied in the last few decades[9-17]. It has been found that back diffusion of the generated CO is the main origin of C contamination in Si feedstock. Accumulation of C in the melt must be investigated according to the transient feature of the CZ-Si process. Bornside et al.[13] derived a chemical model for coupled CO and SiO from thermodynamic analysis of their reactions in the high temperature range. Based on this chemical model, Gao et al.[14] developed a coupled transport model for SiO and CO in argon (Ar) gas, and C and O in a Si melt. However, the C content predicted under the quasi-static assumption does not account for C accumulation during

*1 Research Institute for Applied Mechanics, Kyushu Univ.

CZ-Si crystal growth[11]. Transient global simulations of heat and mass transport have been performed for C accumulation in the melting process of CZ-Si crystal growth[16, 17]. However, in these studies, packed Si chunks were modeled with the thermal conductivity of bulk Si. The difference between the thermal conductivities of packed Si chunks and bulk Si can result in unreliable prediction of the thermal history of the melting process.

The present study focuses on evolution of C contamination during the melting process of packed Si chunks in CZ-Si crystal growth. The heat transport modeling took into account the ETC of packed Si chunks, which is affected by the packing structure, as a function of the chunk size and porosity. The ETC model proposed by IAEA[8] was applied in the transient global simulation of the melting process. The effect of the chunk size on the melting process and C accumulation were analyzed by parametric studies of different packing structures.

2.　Modeling and Formulations

The methodology for transient global simulation of the coupled heat and mass transport during the melting process of CZ-Si crystal growth has been reported elsewhere[16]. A virtual proportional integral derivative (PID) controller for the temperature [18] was introduced to realize power control of the heater. The coupled boundary conditions for the transport of impurities were modeled based on the chemical reactions in a CZ-Si crystal furnace.
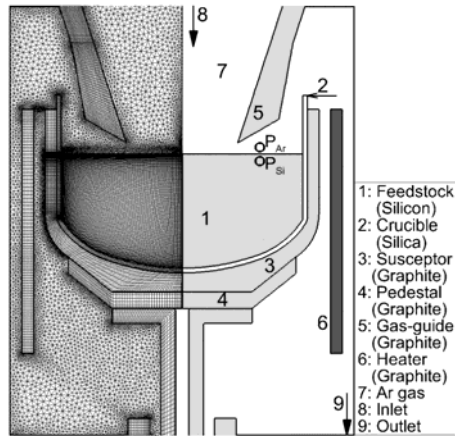

Fig. 1 Configuration and grids used to simulate the melting process of CZ-Si crystal growth.

The configuration of the system and the computational grids for the melting process of CZ-Si crystal growth are shown in Fig. 1. The furnace was divided into a number of domains and a structured mesh was generated for the solid and Si feedstock domains, while an unstructured mesh was applied for the Ar gas domain. The furnace is described in detail in Ref. 16). In order to simplify the transient global modeling, the volume of Si domain was kept constant, and set the density as bulk Si or melted Si according to its phase

state. The results at two locations in the gas domain and Si domain (labeled as P_{Ar} and P_{Si}, respectively) were monitored during the transient global simulation, as shown in Fig. 1.

2.1　IAEA model for the ETC of packed Si chunks

In the idealized packing structure, heat is simultaneously transported by four mechanisms: radiation in the void region, conduction of the gas, conduction of spheres, and convection of the gas. The heat flux is considered to consist of three parts excluding convection: a solid conduction–void radiation–solid conduction process, a solid conduction–gas conduction–solid conduction process, and a solid conduction–contact area conduction–solid conduction process. Therefore, the following three different types of effective conductivity must be evaluated: void radiation plus solid conduction (k_e^r), gas conduction plus solid conduction (k_e^c), and contact conduction plus solid conduction (k_e^c). The total effective conductivity is the sum of these three parts [6]:

$$k_{eff} = k_e^r + k_e^g + k_e^c \qquad (1)$$

Definitions of these three parts can be found in IAEA-TECDOC-1163[8], which was validated by experimental data for the entire temperature range.

In addition, a porosity function must be applied for the packed Si chunks [19]:

$$\varepsilon(\delta) = \varepsilon_\infty \left[1 + (1 - \varepsilon_\infty) \exp(-6\delta) / \varepsilon_\infty \right] \qquad (5)$$

where ε_∞ is the bulk porosity of the homogeneous domain and δ is the dimensionless wall distance $\Delta L / d_p$, where ΔL is the wall distance.

At the top surface of the Si feedstock, the boundary condition of thermal equilibrium is

$$k_{eff} \frac{\partial T}{\partial n} = \sigma_{SB} E_{eff} \left(T^4 - T_{env}^4 \right) \qquad (6)$$

where　is the effective emissivity of the packed Si chunks, which is given by the fitted function[20].

$$E_{eff} = E_S \left\{ 1 - 0.95 \exp\left[-1000 d_p \varepsilon (1 - E_S) \right] \right\} . \qquad (7)$$

where E_S is the emissivity of Si and d_p is the equivalent diameter of the Si chunks.

2.2　Reactions and deposition on the surface of Si chunks

The chemical reactions and transport mechanisms of the species during the melting process in CZ-Si growth are shown schematically in Fig. 2. The coupled boundary conditions for the transport of impurities were modeled based on the following six reactions that occur in a CZ furnace:
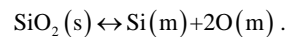
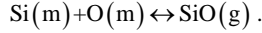(1) Crucible/susceptor interface:

$SiO_2(s) + C(s) \leftrightarrow CO(g) + SiO(g)$.
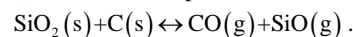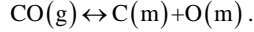
(2) Graphite fixture surfaces:

$SiO_2(s) + C(s) \leftrightarrow CO(g) + SiO(g)$.
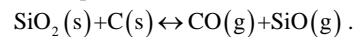
(3) Melt/crucible interface:

$SiO_2(s) \leftrightarrow Si(m) + 2O(m)$.

(4) Gas/Si interface (for O):

$Si(m)+O(m) \leftrightarrow SiO(g)$.

(5) Gas/Si interface (for C):

$CO(g) \leftrightarrow C(m)+O(m)$.

(6) Gas/Si interface (for SiC):

$2Si(s/m)+CO(g) \leftrightarrow SiC(s)+SiO(g)$.
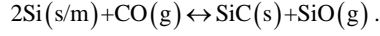
In the above equations, (s) denotes a solid, (m) denotes a melt, and (g) denotes a gas. These coupled boundary conditions were defined and implemented in the same manner as in Ref. 16).
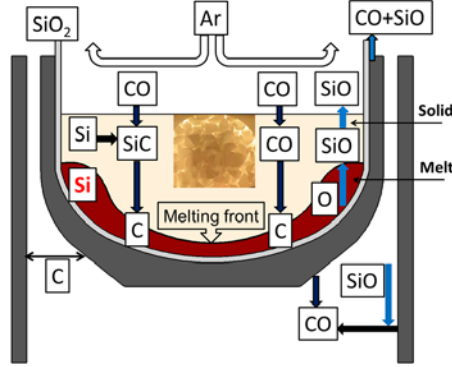

Fig. 2 Schematic of the transport of the species during the melting stage of CZ-Si crystal growth.

Si chunks and melted Si coexist in the crucible during the melting process. Reactions (4)–(6) are involved at the gas/Si interface and in the unmelted Si feedstock. To investigate the surface reaction and deposition, a simplified model for SiC generation by the reaction between CO and Si was used for the surface of the packed Si chunks[17]. O, C, SiO, CO, and SiC coexist in the unmelted Si feedstock and at the gas/Si interface. In reaction (6), CO is consumed and SiO is generated in the solid Si feedstock. Unmelted Si is defined as the buffer between the melt and the gas. SiO and CO diffuse in this porous media with effective diffusion coefficients.

The block-shaped Si feedstock was assumed to be equivalent to identical spheres with FCC packing and porosity of $1-\left(\pi/\sqrt{18}\right)$. Under this assumption, gaseous SiO and CO can penetrate into the porous Si feedstock. Deposition of SiC on the surfaces of the blocky Si feedstock was modeled using a volume generation source:

$$G_{SiC} = K_{SiC} A_V \left(C_{CO} - C_{CO}^0 \right), \qquad (8)$$

where K_{SiC} is the reaction equilibrium constant ($K_{SiC} = \exp\left(9610/T-3\right)$), A_V is the specific surface area (by volume), and $\left(C_{CO} - C_{CO}^0\right)$ is the increase in the CO content. Diffusion transport of CO and SiO in void areas was assumed to be dominated by the effective diffusion coefficient:

$$D_{eff} = D_{Ar}\varepsilon ,$$

(9)

where D_{Ar} is the diffusion coefficient in Ar gas. The

reaction between gaseous CO and solid Si was assumed to occur in a similar way to the process that occurs in a packed-bed reactor. The generated SiC was assumed to dissolve in the melt as C and Si atoms until the C concentration reached the limit of the solubility of C. Finally, C contamination in the melted Si feedstock from dissolution of SiC can be predicted.

The other boundary conditions for the Ar gas and Si headstock were as follows. A zero-flux boundary condition was used for C at the crucible wall. Zero SiO and CO fluxes were used for the non-C walls and the symmetry axis in the gas. The SiO and CO concentrations were set to zero for the gas inlet. Zero SiO and CO gradients were used for the gas outlet.

3.   Results and discussion

Incorporation of C from the gas/melt interface proceeds from the melting stage to the tailing stage. According to accumulation of C in the Si feedstock, the thermal history, processing duration, and Ar gas flow pattern are the key factors for C reduction. The accumulation process of C can only be predicted by transient global simulation. Therefore, a set of transient global simulations was performed for the melting process of CZ-Si crystal growth with different packing structures. The thermal field, melt and gas flow, and transport of the species were dynamically predicted using fully coupled boundary conditions for the heat, flow, and species. The reference values of furnace pressure and Ar gas flow rate were set to 15 Torr and 10 SLPM (standard liter per minute at 273.15 K and 760 Torr), respectively. Packed Si chunks were modeled by the closest packing of identical spheres with the ETC model from the IAEA. The porosity function with a bulk porosity of 0.26 was involved in the ETC model for every case. Porosity and chunk size were included only in the ETC model but not the control volume and mass of transport equations. The heights of solid and melt were also set with identical value, with the weight about 120 kg of bulk Si. A top layer with the thickness of 50 mm was set as the area of interest.

3.1 Relationship between the ETC and the Si chunk size or porosity
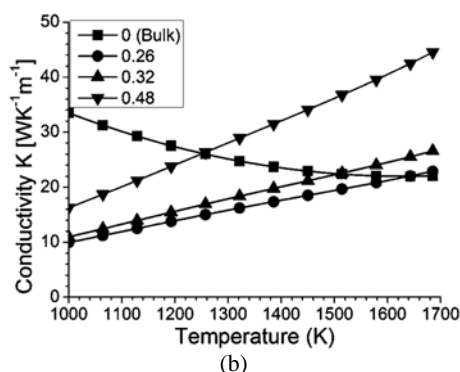

(a)

(b)
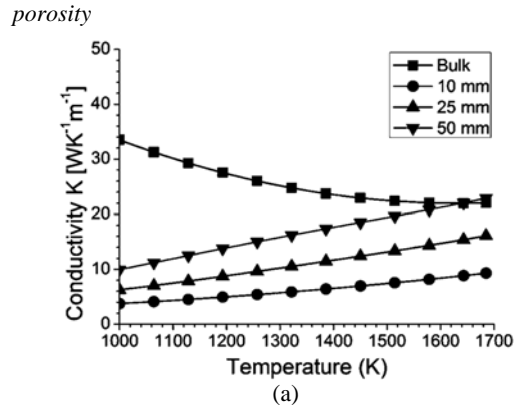
Fig. 3 ETC profiles for (a) different sized Si chunks and (b) different porosities of the packing structure.

To investigate the effect of the packing structure of Si on the melting process, two of the important parameters of the ETC model were considered: the chunk size and the porosity. Because the ETC is a function of the packing structure and the temperature, the ETCs for different porosities and different chunk sizes were plotted for a wide temperature range. Comparison of the ETC profiles for different sized chunks is shown in Fig. 3(a) with a constant porosity of 0.26. The thermal conductivity of bulk Si is always higher than the ETCs for different chunk sizes except in the high temperature range. Thus, the difference between the conductivities has to be taken into account by the ETC model of packed Si chunks. Increasing the chunk size resulted in an increase of the ETC, as well as the temperature. These trends are related to the thermal radiation contribution of the ETC model, which is proportional to $4\sigma d_p T^4$. At high temperatures, thermal radiation among chunks dominates the heat transport in the packed Si feedstock. Comparison of ETC profiles for different porosity packing structures is shown in Fig. 3(b) with a constant equivalent diameter of 50 mm. With increasing porosity, the ETC increases and exceeds the conductivity of bulk Si in the high temperature range. Thermal radiation is also enhanced by the increase of the void space between packed Si chunks. Because the ETC model is fully coupled with the temperature, it is believed that the chunk size and porosity of packed Si could affect the thermal history of melting.

3.2 Effect of the ETC model on the melting duration and C contamination

With the effective conductivity model, a transient global simulation of heat and mass transport was performed for the entire melting process with the ETC model. PID control[18] of the temperature at the heater was implemented by manipulating the heating power. The heater temperature reached the set point (1835 K) from its initial state in 4 h. The Si feedstock in the crucible melted and then stabilized for the next stage. The temperature at the top center of the Si feedstock was monitored as indicator of the fully melted state.

The heater power profiles and the monitored Si temperature are plotted in Fig. 4 with the ETC model (porous Si chunks) and without the ETC model (ideal bulk Si). Application of the ETC model leads to significant differences in the heating power and melting duration for identical setting temperature profiles of the heater. This indicates that the effect of porous Si on the thermal history cannot be ignored when modeling the melting process.
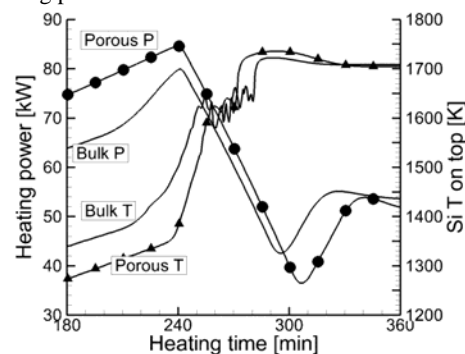

Fig. 4 Power profiles and temperature evolution by the thermal conductivity of bulk Si and the ETC model of porous Si.
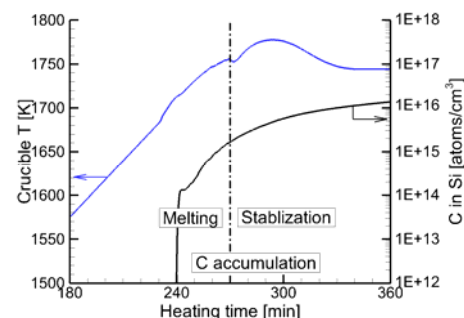

Fig. 5 Temperature evolution of the crucible wall and the C concentration of the monitoring point in the Si feedstock.

The temperature at the end of the vertical crucible wall was monitored as judgment of the melting start. CO incorporated into Si as C from the melt surface. The monitored crucible temperature and the C concentration in the Si feedstock temperature are plotted in Fig. 5. C contamination before melting is insignificant. C accumulation started from the melting stage, and lasted until the stabilization stage. This plot indicates that most C contamination comes from the stabilization stage owing to the larger incorporation area.

3.3 Effect of the chunk size on the melting duration and C contamination

A top layer with the thickness of 50 mm was set as the area of interest to investigate the chunk size effect on the melting process and C accumulation. The layer of interest was replaced by smaller chunks with diameters of 10 and 25 mm. Small chunks packed in the upper part of the layer can

reduce the total time of the melting process, as shown in Fig. 6(a). For the 10 mm chunks, the durations of melting and stabilization were both shorter than those for the 50 mm chunks. The total duration of melting and stabilization was shortened by the decrease of Si chunk size in the interested layer. Comparison of the power profiles and temperature evolution are shown in Fig. 6(b). Smaller Si chunks packed in top part smoothed the power profile and sped up the melting process. This is because heat loss at the top surface follows the heat flux boundary condition, the heat balance between conduction flux and radiation flux (Eq. 6). Small Si chunks result in lower ETC and effective emissivity. Loading small chunks in the upper part of the layer can reduce heat loss because of the lower ETC and effective emissivity.
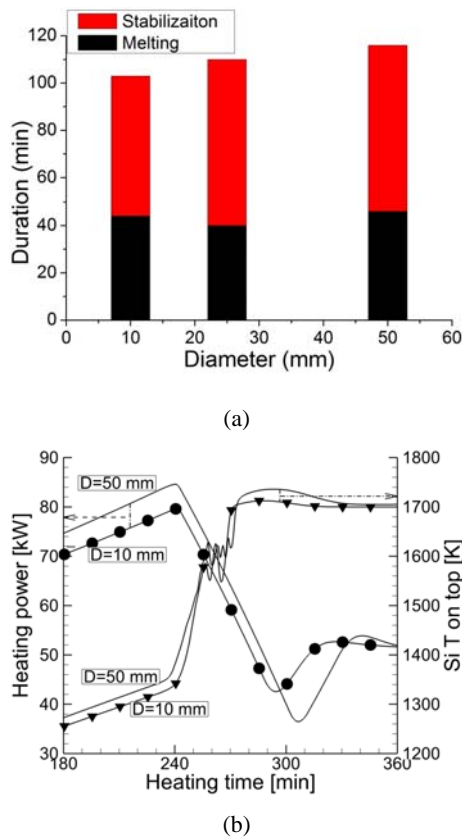

(a)

(b)

Fig. 6 Effect of the chunk size on the melting process. (a) Duration of melting (black) and the stabilization stage (red) for different chunk sizes and (b) power profiles and temperature evolution for 10 and 50 mm chunks.

The effect of the packing structure on C contamination was also investigated in the melting and stabilization stages. The concentration of C in melted Si is compared for 50 mm and 10 mm chunks in Fig 7(a). Small Si chunks packed in the top part of the layer resulted in much lower C contamination. The final C concentrations after the stabilization stage for these two cases are shown in Fig. 7(b). With 10 mm Si chunks packed in the upper part of the layer, the total C concentration decreased by 24% after melting, while there

was a 36% decrease for the final C concentration of the melting process. Therefore, small chunks packed in the upper part of the layer can reduce C accumulation in Si by speeding up the melting process.
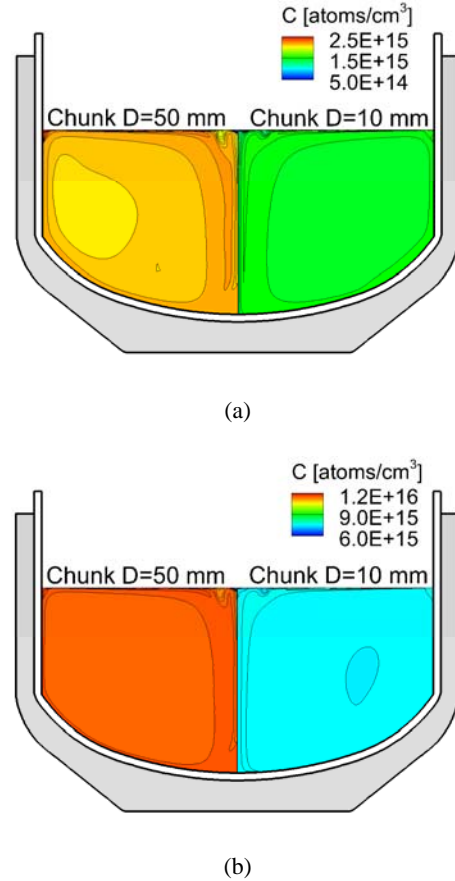

(a)

(b)

Fig. 7 Effect of the chunk size on C accumulation. (a) C accumulation during the melting stage and (b) C accumulation during the stabilization stage for 50 (left) and 10 mm (right) chunks.

4. Conclusion

To investigate C contamination prior to the growth stage of CZ-Si crystal growth, transient global simulations of heat and mass transport were performed for the melting process of CZ-Si with different packing structures of Si chunks. The heat transport modeling took into account the ETC of the packed Si chunks, which depends on the parameters of the packing structure. The ETC model proposed by IAEA was used in the melting process prediction of packed Si. Parametric studies of different packing structures indicate that heat transport in the crucible is affected by the ETC and the emissivity of the Si feedstock. It was found that smaller Si chunks packed in the upper part of the layer can speed up the melting process and smooth the power profile by heat loss reduction. Decrease in the durations of melting and the stabilization stage resulted in reduction of C accumulation in the Si feedstock. Optimization of the melting process by the

packing structure is possible and essential for C reduction in CZ-Si crystal growth. Random packing of irregular shaped and various sizes of Si chunks or granules needs to be investigated to determine the generality of the findings.

Acknowledgment

References

1) K. Seigô, M. Yoshiaki, K. Masaru, I. Takashi, Thermally induced microdefects in Czochralski-grown silicon: nucleation and growth behavior, Jpn. J. Appl. Phys., 21 (1982), pp. 1-12.

2) Y. Nagai, S. Nakagawa, K. Kashima, Crystal growth of MCZ silicon with ultralow carbon concentration, J. Cryst. Growth, 401 (2014), pp. 737-739.

3) L. Raabe, O. Pätzold, I. Kupka, J. Ehrig, S. Würzner, M. Stelter, The effect of graphite components and crucible coating on the behaviour of carbon and oxygen in multicrystalline silicon, J. Cryst. Growth, 318 (2011), pp. 234-238.

4) U. Martini, L. Bonanno, P. Collareta, M. Porrini, Method of loading a charge of polysilicon into a crucible, in, Google Patents, 2014.

5) W. van Antwerpen, C.G. du Toit, P.G. Rousseau, A review of correlations to model the packing structure and effective thermal conductivity in packed beds of mono-sized spherical particles, Nucl. Eng. Des., 240 (2010), pp. 1803-1818.

6) W. Van Antwerpen, Modelling the effective thermal conductivity in the near-wall region of a packed pebble bed, in, North-West University, Potchefstroom, South Africa, 2009.

7) R. Bauer, E.U. Schluender, Effective radial thermal conductivity of packings in gas flow. Part II. Thermal conductivity of the packing fraction without gas flow, International Journal of Chemical Engineering, 18 (1978), pp. 189-204.

8) I.A.E. Agency, Heat transport and afterheat removal for gas cooled reactors under accident conditions, in, International Atomic Energy Agency (IAEA), Vienna, 2001, pp. 301-304.

9) H.M. Liaw, Oxygen and carbon in Czochralski-grown silicon, Microelectronics Journal, 12 (1981), pp. 33-36.

10) B.O. Kolbesen, A. Mühlbauer, Carbon in silicon: Properties and impact on devices, Solid-State Electron., 25 (1982), pp. 759-775.

11) R.W. Series, K.G. Barraclough, Control of carbon in Czochralski silicon crystals, J. Cryst. Growth, 63 (1983), pp. 219-221.

12) T. Fukuda, M. Koizuka, A. Ohsawa, A Czochralski silicon growth technique which reduces carbon to the order of 1014 per cubic centimeter, J. Electrochem. Soc., 141 (1994), pp. 2216-2220.

13) D.E. Bornside, R.A. Brown, T. Fujiwara, H. Fujiwara, T. Kubo, The effects of gas-phase convection on carbon contamination of Czochralski-grown silicon, J. Electrochem. Soc., 142 (1995), pp. 2790-2804.

14) B. Gao, K. Kakimoto, Global simulation of coupled carbon and oxygen transport in a Czochralski furnace for silicon crystal growth, J. Cryst. Growth, 312 (2010), pp. 2972-2976.

15) A.N. Vorob'ev, A.P. Sid'ko, V.V. Kalaev, Advanced chemical model for analysis of Cz and DS Si-crystal growth, J. Cryst. Growth, 386 (2014), pp. 226-234.

16) X. Liu, B. Gao, K. Kakimoto, Numerical investigation of carbon contamination during the melting process of Czochralski silicon crystal growth, J. Cryst. Growth, 417 (2015), pp. 58-64.

17) X. Liu, B. Gao, S. Nakano, K. Kakimoto, Numerical investigation of carbon and silicon carbide contamination during the melting process of the Czochralski silicon crystal growth, Cryst. Res. Technol., 50 (2015), pp. 458-463.

18) Y. Lee, J. Lee, S. Park, PID controller tuning for integrating and unstable processes with time delay, Chem. Eng. Sci., 55 (2000), pp. 3481-3493.

19) M.L. Hunt, C.L. Tien, Non-darcian flow, heat and mass transfer in catalytic packed-bed reactors, Chem. Eng. Sci., 45 (1990), pp. 55-63.

20) J. Yamada, Y. Kurosaki, T. Nagai, Radiation Heat Transfer Between Fluidizing Particles and a Heat Transfer Surface in a Fluidized Bed, J. Heat Transfer, 123 (2001), pp. 458-465.